Persistent Na^+ current couples spreading depolarization to seizures in *Scn8a* gain of function mice

Isamu Aiba, Yao Ning, Jeffrey L. Noebels

Abstract

Spreading depolarization (SD) is a slowly propagating wave of massive cellular depolarization that transiently impairs the function of affected brain regions. While SD typically arises as an isolated hemispheric event, we previously reported that reducing M-type potassium current (I_{KM}) by ablation of *Kcnq2* in forebrain excitatory neurons results in tightly coupled spontaneous bilateral seizure-SD complexes in the awake mouse cortex. Here we find that enhanced persistent Na^+ current due to gain-of-function (GOF) mutations in *Scn8a* (N1768D/+, hereafter D/+) produces a similar compound cortical excitability phenotype. Chronic DC-band EEG recording detected spontaneous bilateral seizure-SD complexes accompanied by seizures with a profound tonic component, which occurs predominantly during the light phase and were detected in the mutant mice across ages between P40-100. Laser speckle contrast imaging of cerebral blood flow dynamics resolved SD as bilateral wave of hypoperfusion and subsequent hour-lasting hypoperfusion in $Scn8a^{D/+}$ cortex in awake head-restrained mice subjected to a subconvulsive PTZ. Subcortical recordings in freely moving mice revealed that approximately half of the spontaneous cortical seizure-SD complexes arose with concurrent SD-like depolarization in the thalamus and delayed depolarization in the striatum. In contrast, SD-like DC potential shifts were rarely detected in the hippocampus or upper pons. Consistent with the high spontaneous incidence *in vivo*, cortical slices from $Scn8a^{D/+}$ mice showed a raised SD susceptibility, and pharmacological inhibition of persistent Na^+ current (I_{NaP}), which is enhanced in $Scn8a^{D/+}$ neurons, inhibited SD generation in cortical slices *ex vivo*, indicating that I_{NaP} contributes to SD susceptibility. *Ex vivo* Ca^{2+} imaging studies using acute brain slices expressing genetic Ca^{2+} sensor (Thy1-GCAMP6s) demonstrated that pharmacological activation of I_{KM} suppressed Ca^{2+} spikes and SD, whereas I_{KM} inhibitor drastically increased the frequency of Ca^{2+} spikes in the hippocampus of $Scn8a^{D/+}$ mice, but not in WT, suggesting that I_{KM} restrains the hyperexcitability resulting from *Scn8a* GOF mutation. Together, our study identifies a cortical SD phenotype in *Scn8a* GOF mice shared with the *Kcnq2*-cKO model of developmental epileptic encephalopathy and reveals that an imbalance of non-

inactivating inward and outward membrane currents bidirectionally modulates spatiotemporal SD susceptibility.

Author affiliations:

Department of Neurology, Baylor College of Medicine Houston TX 77030

Running title: Spreading depolarization in Scn8a GOF mice

Keywords

Epilepsy; Nav1.6; tonic seizure;

Introduction

Spreading depolarization (SD) is a slowly propagating wave of cellular depolarization of focal origin, involving minute-lasting profound intra/extracellular ionic gradient, massive tissue edema, hypoxia, and transient loss of neuronal activity.[1,2] Clinical studies reveal frequent SD incidence in traumatic and vascular brain injuries, and SD events can be independently or additively associated with neurological deficits. In epilepsy cases, peri-ictal and interictal SD may contribute to neurosensory (headache/allodynia, photophobia) and behavioral (depression, anxiety) comorbidities. However, due to the necessity for intracranial recordings, most of the evidence linking SD with these symptoms is only available from clinical observation of acute brain injury patients under critical care or experimental models using exogenously provoked SD, often under sedation. The pathological significance of SD in epilepsy patients has yet to be clarified in awake ambulatory settings.

In recent experimental studies using chronic DC-band intracranial EEG recording, we found that conditional deletion of *Kcnq2*, a gene frequently mutated in developmental epileptic encephalopathy (DEE),[3,4] in mouse forebrain excitatory neurons (Emx1-Cre:*Kcnq2* flox/flox; hereafter Emx-Kcnq2 cKO) increases tissue SD susceptibility and results in spontaneous bilateral cortical seizure-SD co-generation.[5] *Kcnq2* encodes the potassium channel pore-forming subunit responsible for the M-type K^+ current (I_{KM}), a non-inactivating slow outward current enriched in the axonal initial segment (AIS).[6,7] At the AIS, *Kcnq2*/Kv7.2 forms a heterotetramer with *Kcnq3*/Kv7.3 and regulates local electrogenesis by counteracting depolarizing voltage-gated Na^+ currents.[8] This compartmental functional proximity as well as their similar kinetics raises the possibility that increased persistent sodium current (I_{NaP}) in the excitatory neurons may produce an intrinsic membrane excitability defect equivalent to that seen in *Kcnq2*-cKO mice.

In the mammalian brain, *SCN2A*/Nav1.2 and *SCN8A*/Nav1.6 are the major voltage-gated Na^+ channel (VGSC) pore-forming subunits expressed in the postnatal forebrain excitatory neurons. While both channels are enriched in the AIS,[9] *SCN8A*/Nav1.6 in particular makes a dominant contribution to I_{NaP}.[10–12] Gain-of-function (GOF) mutations in *SCN8A* associated with enhanced I_{NaP} have been identified in developmental epileptic encephalopathy patients,[13,14] and a knock-in mouse carrying a heterozygote *Scn8a* N1768D (hereafter $Scn8a^{D/+}$)[15] shows enhanced persistent

and resurgent Na^+ current in excitatory neurons[16] and recapitulates major features of the DEE phenotype including spontaneous seizures, behavioral abnormality, and premature death.

In this study, we characterized SD events in *Scn8a*$^{D/+}$ mice to elucidate the role of I_{NaP} in SD regulation. As hypothesized, chronic EEG monitoring of these mice detected spontaneous bilateral seizure-SD complexes, as previously detected in *Kcnq2*-cKO mice.[17] Furthermore, laser speckle contrast imaging (LSCI) resolved synchronous bilateral propagation of cortical hypoperfusion associated with the SD wave, and subcortical EEG recordings indicated frequent involvement of the thalamus and striatum. Additionally, *ex vivo* assay revealed increased SD susceptibility in acutely prepared *Scn8a*$^{D/+}$ cortical slices which was suppressed by I_{NaP} inhibitors riluzole and GS967. Together, our study reveals an SD phenotype arising from a clinically identified *Scn8a* GOF mutation and demonstrates that an imbalance of persistent Na^+ and K^+ currents produces similar patterns of SD susceptibility in genetic mouse DEE models.

Materials and methods

Animals

All experiments were conducted under the protocol AN8446 approved by IACUC of Baylor College of Medicine. *Scn8a*$^{D/+}$ mice were originally generated [15] and kindly provided by Dr. Miriam Meisler (University of Michigan). These mice were crossed once with the C57BL6J line at Baylor College of Medicine and the offspring was maintained by inbreeding. In some experiments, *Scn8a*$^{D/+}$ mice were crossed with a Thy1-GCAMP6s GP4.3 mouse (JAX# 024275)[18] for Ca^{2+} imaging studies. All mice were maintained on a 12-hour light-dark cycle with ad libitum access to water and standard chow (5V5M).

Surgery

Mice received preoperative analgesia (2 mg/kg meloxicam, 1 mg/kg buprenorphine extended release, s.c.), followed by 2-3% isoflurane anesthesia, and were placed on a stereotaxic frame with a heating pad. The incision site was depilated and cleansed with betadine and 70% ethanol three times, and locally injected with a 2% lidocaine/0.5% bupivacaine mixture. The cranial surface was

exposed, and 0.5 mm burr holes were made for insertion of a 0.1 mm Teflon insulated silver wire either in the epidural space for cortical surface recording or into subcortical structures, using the following coordinates relative to the bregma; cortex (Anterior ±1.0 mm/Lateral: +1.5 mm), hippocampus (Anterior -1.5mm, Lateral 1.0 mm, depth 2 mm), striatum (Anterior +0.5 mm/Lateral +1.0 mm, depth 2-2.5 mm), thalamus (Anterior -1.5 mm, Lateral 1.0 mm, depth 3.5-4 mm). For the implantation in the dorsal pons, bilateral craniotomies (Anterior: -1.0 mm, Lateral: 1.5 mm, relative to lambda) were made to visually identify and avoid blood vessels over the inferior colliculus when inserting the electrode wire. The tips of depth electrodes were marked with DiD fluorescent dye. A ground electrode was placed over the cerebellum through an occipital bone burr hole. The exact positions of the burr holes were adjusted by ~1 mm when major blood vessels were present. All wires were connected to an 8-channel pedestal on the skull and cemented with Metabond.

For LSCI studies, the entire dorsal skull was exposed, and epidural electrodes were placed over the somatosensory cortex, olfactory bulb, and cerebellum (ground). A head-bar was placed on the occipital bone. After securing each component using Metabond, the skull surface was coated with cyanoacrylate 3 times.

After the surgery, mice were returned to the vivarium and received postoperative analgesia (2 mg/kg Meloxicam, s.c.) for 3 days, with further recovery for at least 5 days before monitoring. The locations of depth electrodes were verified following recordings by visualizing the fluorescently marked wire tip.

Chronic EEG monitoring

Mice were transferred to a satellite room where temperature is maintained at 22-24 °C and humidity 40-70% with a 12-hour light-dark cycle. Each mouse was connected to a tethered wire (1 mm diameter) in a recording chamber. DC-EEG signals were amplified with a Bioamp (ADI) along with video using LabChart software (ADI). During monitoring, mice had ad libitum access to water and food, and beddings were replaced every week.

SDs were first screened based on the voltage and duration thresholds (>5 mV, 30 seconds) and each event was later visually confirmed. A tonic seizure was defined as the chaotic high-frequency

EEG activity associated with tonic posturing. In a subset of subcortical recordings, events in one hemisphere were excluded from analysis when depth electrodes were not properly located in the targeted site or the EEG baseline was not stable enough to analyze a DC potential shift.

LSCI in awake head-restrained mice

Mice were placed on a treadwheel using a metal bar head restraint. The dorsal surface of the skull was illuminated with an 800 nm LED (1-2 mW) through a series of lenses to enhance the speckle pattern, and images acquired with a CMOS camera (DMK 33UX273) fitted with an IR-pass filter and polarizer. A temporal contrast image was generated from fifteen serially captured images acquired at 50 Hz using MATLAB at 1 Hz. The contrast values were used as a measurement of cerebral blood flow (CBF). EEG and EMG signals were obtained (Bioamp). A thermistor (36AWG, 5TC-TT-K-36-36-ROHS, Omega) was used to capture nasal airflow. Overall movement was monitored using a standard CMOS camera through an IR cut filter.

SD was provoked by an intraperitoneal injection of pentylenetetrazol (PTZ) at a subconvulsive dose determined in pilot studies using separate cohorts (titrated from 20 mg/kg in *Scn8a*$^{D/+}$ and 40 mg/kg in WT). SD responses in some mice were examined repetitively, in which case each injection was separated by 5-10 days to minimize any kindling effect.

***Ex vivo* SD studies using acute brain slices**

Acute slices and solutions were prepared as described previously.[17] In brief, mice were deeply anesthetized with ketamine/xylazine mixture, cardiac perfused with NMDG-based dissection solution, and decapitated. The brain was extracted into the dissection solution and sectioned into either coronal somatosensory slices (300 μm thick) containing barrel cortex for KCl-SD assays, or horizontal cortico-hippocampal slices without the barrel cortex for Ca^{2+} imaging. Once cut, slices recovered for 5 minutes in the dissection solution at 35°C and were maintained in ACSF at room temperature.

For *ex vivo* SD threshold analyses, slices were transferred to a submerged chamber (RC-27, Warner Instruments) continuously perfused with ACSF at 2.5 mm/min and maintained at 33-34°C.

The slices were monitored with a CMOS camera (Hamamatsu) for intrinsic optical signal (IOS) and fluorescence imaging. All optical components were controlled with μManager software (https://micro-manager.org/). Field potentials were acquired with glass micropipettes filled with ACSF, amplified by a MultiClamp 700B, and digitized (Digidata 1550B, Molecular devices).

In the KCl SD threshold test, the IOS was acquired at 0.5 Hz while slices were exposed to ACSF containing incrementally elevated KCl concentrations, starting with 6 mM, and incremented by 1 mM every 5 minutes until an SD was detected, as in our previous study.[17]

In the slice Ca^{2+} imaging study, GCAMP6s fluorescence was excited using a Lambda-DG4 (Sutter) at 1 Hz. Spontaneous seizure-like activity and SD were induced by exposure to nominally Mg^{2+} free ACSF (0 mM $MgSO_4$) described in our previous study.[19] In order to minimize the anatomical variation, we chose slices containing the hippocampal fornix. The raw fluorescence images were converted to $\Delta F/F_0$ and analyzed using ImageJ software. Ca^{2+} activities corresponding to seizure-like activities and SD were initially defined based on their correlation with the field potential and were later determined based on the intensity, duration, and migration speed of the Ca^{2+} activity. The Ca^{2+} spike frequency was determined based on the number of Ca^{2+} spikes above the threshold (3 times the standard deviation) during exposure to Mg^{2+}-free solution while excluding the duration of SD.

Drugs

ICA 110381, Riluzole, and XE991 were purchased from Tocris, and GS967 from AOBIOUS. In *ex vivo* studies, drugs were dissolved in DMSO at 100 mM, added to ACSF, and dissolved by sonication. All other chemicals were purchased from Sigma.

Statistics

In bar graphs, data are presented as mean ± standard deviation with individual data points. All data analyses are performed using Labchart, MATLAB, pClamp10, R, and, prism software. The method and result of statistical analysis in each data are described in the corresponding figure

legends. The sample number was predetermined based on previous studies. Experiments were blindly performed where it is possible.

Data availability

Data supporting the findings of this study are available within the article and its Supplementary material. All supporting data in this study are available from the corresponding author on request.

Results

A bilateral seizure-SD complex is the predominant EEG abnormality in *Scn8a*$^{D/+}$ mice

We characterized the cortical SD phenotype in a total eleven *Scn8a*$^{D/+}$ mice (4 males and 4 females *Scn8a*$^{D/+}$ mice, and three male *Scn8a*$^{D/+}$:Thy1GCAMP6s) with chronic DC-band EEG recordings starting from the age of P33-80. Each mouse was implanted with four cortical surface electrodes (**Figure 1A**). During the initial week of recording, almost all generalized seizures were followed by a large negative DC potential shift nearly simultaneously detected at all four electrodes (**Figure 1B**), similar to an EEG event frequently seen in Emx1-*Kcnq2* cKO mice.[17] The DC potential shifts at the anterior and posterior electrodes were similar in amplitude (14.9 ± 7.5 mV vs 16.0 ± 8.6 mV, p=0.4, n=71) and duration (58.3 ± 28.9 s vs 63.4 ± 24.3 s, p=0.26, n=71).

During the recording, five mice started to show irregular DC potential shifts and/or SDs detected only unilaterally (**Figure 1D**, Unilateral Seizure-SD). In these mice, the DC potential shift eventually became undetectable, leaving only a mostly electrographic seizure signature (**Figure 1D**, Seizure) which tended to involve less robust motor manifestations and were not always apparent without EEG. In four of these mice, seizure frequency increased and eventually evolved into status epilepticus (by definition less than an hour interictal interval, **Figure 1D**). One of these mice did not recover and died, while one required euthanasia.

Bilateral seizure-SD complexes and solitary seizures were the major EEG events whose mean frequencies were less than once per day (**Figure 1C**). However, these events tended to appear as a cluster and multiple events could be detected in a single day (see **Figure 1A**). Both seizure-SD

complexes and seizures showed a circadian rhythm; these events were more frequent during the light phase than in the dark phase with slightly distinct peaks (seizure-SD peak at 15.9, seizure peak at 11.4, **Figure 1E**).

Seizure-SD complexes were accompanied by tonic seizures

Each seizure-SD complex was always associated with a generalized motor seizure featuring a robust tonic component characterized by a hunched back with a spastic extension of both fore- and hind limbs as reported in the original characterization of this transgenic mouse.[15] An example of the seizure-SD complex is presented in **Figure 2**. On EEG, the tonic seizure phase was detected as chaotic high-frequency activity, possibly contaminated by muscle artifact, which is preceded or followed by a slower sharp wave seizure activity associated with clonus (**Figure 2B**, Ictal). These tonic seizures were present at the onset of a negative DC potential shift of SD (**Figure 2B**), and one or two additional recurrent tonic seizures were detected after recovery of the DC potential shift in 66.6% of events (**Figure 2D**). The slow baseline drift and the subsequent sharp spikes seen in the high-pass filtered trace (**Figure 2B**) are nearly identical to the electrographic seizure characterized using an AC-coupled amplifier,[15] reinforcing the necessity of unfiltered DC amplification for reliable detection of SD. The peak of the DC potential shift was followed by a minutes-lasting depression of EEG amplitude (see High-pass trace, and power spectrum in **Figure 2A**), while it could be interrupted by tonic seizures (**Figure 2C**). Tonic seizures were occasionally detected during animal handling, while they were rarely detected in the absence of cortical seizure or seizure-SD complex during chronic monitoring.

In a few instances, we detected a DC shift that preceded the tonic seizure. This is likely due to SD initiation near the recording site and implies that seizure and SD may not always propagate as a complex, or that an EEG seizure is not a necessary trigger of SD in this model.

Tonic spasm during audiogenic seizure does not involve cortical SD

Next, we examined whether cortical SD is present during the tonic spasm during an audiogenic seizure in *Scn8a*$^{D/+}$ mice. In awake young *Scn8a*$^{D/+}$ mice (P30-45), a loud buzzer sound provoked

audiogenic seizures, characterized by wild running followed by sudden motor arrest in an extended tonic spastic posture (**Figure 3**, upper). During the tonic phase, we detected a chaotic high-frequency EEG activity similar to that seen during a spontaneous tonic seizure associated with a seizure-SD complex. In all six recordings, audiogenic seizures were not associated with the robust cortical DC potential shifts suggestive of SD (**Figure 3**, lower). Thus, while chronic monitoring revealed the frequent appearance of tonic seizures with cortical SD, tonic seizures can be triggered as an isolated paroxysmal event without a cortical SD.

Bilateral SD wave detection by LSCI

In order to gain further insight into the pathophysiology of the bilateral SD event, we conducted a LSCI of CBF[20] in head-restrained awake mice. No spontaneous seizure-SD complexes were detected in a total of >30 hours of monitoring from eight *Scn8a*$^{D/+}$ mice. Therefore, we utilized a subconvulsive PTZ injection method which reportedly triggered bilateral SD in non-epileptic awake rats.[21] In Scn8a$^{D/+}$ mice, a subconvulsive PTZ injection (20-30 mg/kg, i.p.) triggered a bilateral slow DC potential shift (16.1 ± 3.0 mV, 79.8 ± 29.4 s, n=8) in 62% (8/13) of trials in five *Scn8a*$^{D/+}$ mice (**Figure 4A&B**). Similar to spontaneous seizure-SD complexes, these SDs were preceded by a brief seizure and visualized as a bilaterally-synchronous wave of cerebral hypoperfusion which always appeared at the lateral edge of the dorsal cortical surface and spread toward the midline (**Figure 4B, Video2**). The wave of hypoperfusion reaches the midline within 15-20 seconds after its appearance (**Figure 4A**), suggesting that SD spread through the cortex at a rate >15 mm/minute. The initial wave of hypoperfusion was followed by a transient partial recovery and subsequently by an hour-lasting hypoperfusion (**Figure 4B**). Similar to spontaneous seizure-SD complexes, PTZ-induced seizure-SD complexes were also accompanied by tonic seizures temporally associated with enhanced EMG signal, respiratory arrest (apnea), and abrupt decrease in CBF (**Figure 4C**). These neurological effects were often followed by massive salivation (**Figure 4C&D**), which often occluded the detection of the nasal airflow. In freely moving mice, we could not determine whether drooling is also present in spontaneous seizure-SD complexes due to the limited facial resolution during chronic monitoring. After recovery from seizure-SD, the mouse typically loses the grip on the wheel along with prolonged immobility (**Figure 4D** postictal).

In the control experiments using WT mice, a higher dose of PTZ (40-60 mg/kg) was required to trigger a brief generalized seizure followed by an SD. In WT, bilateral SD was less common than in *Scn8a*$^{D/+}$ mice, and SDs in the majority of mice (75%, 6/8) were unilateral (**Figure 4E**, Fisher's exact test, p=0.007). SD detected in WT mice had a similar amplitude (**Figure 4F**, 14.5 ± 8.3 mV, n=8, p=0.46), while the duration of DC potential shift was ~40% shorter than in *Scn8a*$^{D/+}$ (**Figure 4G,** 46.9 ± 21 s, n=8, p=0.024), suggesting SD is less intense. None of the evoked SDs in WT mice were associated with robust tonic seizure or apnea (**Figure 4H**), indicating that the paroxysmal tonic spasm associated with SD was a specific feature of *Scn8a*$^{D/+}$ mice. The CBF responses during SD in WT were similar to those of *Scn8a*$^{D/+}$ mice and were also characterized by a wave of hypoperfusion originating at the lateral cortical convexity and spreading toward the midline. While LSCI does not reliably report the absolute CBF dynamics, normalized mean traces suggest similar CBF changes in WT and *Scn8a*$^{D/+}$ mouse cortex (**Figure 4I**).

Together, these results indicate that the *Scn8a* $^{D/+}$ mouse cortex is intrinsically susceptible to bilateral SD *in vivo*. Assuming that the PTZ-evoked SD reproduced spontaneous events, the bilateral spreading pattern and a fast propagation rate of the depolarization wave could explain the near-simultaneous detection of DC potential shift in both anterior and posterior electrodes during chronic monitoring (**Figure 1B**). The propagating pattern also suggests that the bilateral SD wave likely originates from either somatosensory barrel cortex, or even from more distant regions, such as the piriform cortex and amygdala (see Discussion).[22]

Subcortical involvement of seizure-SD complex

Recent studies of a familial hemiplegic migraine type-1 (FHM1) *Cacna1a* knock-in mouse model suggest that a high SD susceptibility is associated with SD invasion into subcortical regions.[23–25] Since the tonic phase of an audiogenic motor seizure is often absent in the cortical EEG and likely mediated by subcortical and brainstem motor pathways, we conducted additional chronic monitoring using bilateral cortical surface and depth electrodes targeting the hippocampus, striatum, thalamus, and upper pons.

1) Hippocampus

SD in the hippocampus was not common in *Scn8a*$^{D/+}$ mice. In the hippocampal recordings, depth electrodes were positioned within CA1 regions or in the dentate gyrus (DG). Slow DC shifts in CA1 stratum radiatum (amplitudes: 20.7 ± 3.0 mV, duration: 49.9 ± 13.0 s) were detected only in a mouse during cortical seizure-SD complexes, and no robust DC potential shifts were detected in the remaining four mice (**Figure 5A**). Overall, intrahippocampal DC potential shifts temporally associated with cortical seizure-SD complex were detected in 17.5% (11/63, total 5 mice) and were relatively rare (but see Discussion). Tonic motor seizures were evident in the hippocampal recordings as a high-frequency activity similar to those detected in the neocortex.

2) Striatum

Delayed SD-like DC potentials were detected in the striatum in association with 36.0% (27/75, total 5 mice) of cortical seizure-SD complexes with a large delay. These DC potential shifts (amplitude: 11.3 ± 6.6 mV, duration: 30.2 ± 13.2 s) appeared with a 144.8 ± 97 s delay (**Figure 5B**). Similar delayed DC potential shifts have been reported, and are considered to be the secondary detection of a cortical SD wave invading the striatum.[26] Tonic seizures were also detected in the striatum as high-frequency activity.

3) Thalamus

Recordings from ventrobasal thalamic nuclei detected large DC potential shifts coincident with 47.8% (28/64, total 5 mice) of cortical seizure-SD complexes (**Figure 5C**). These thalamic depolarizations were large amplitude but shorter-lasting (amplitude: 9.6 ± 4.6 mV, duration: 36.0 ± 20.0 s) than the concurrent cortical DC shift. Tonic motor seizures were detected in the thalamus as a negative DC potential shift with overriding high-frequency activity.

4) Inferior colliculus and rostral pontine nucleus

SD-like DC potentials were rarely detected in the inferior colliculus (n=4 mice) and pontine reticular nucleus (n=2 mice). Robust synchronized ictal discharges were absent in both structures, while unique 2-3 Hz activities were detected in both regions during cortical SD (delayed activity in **Figure 5D**). SD in the inferior colliculus was detected only once in a mouse undergoing a moribund decline in physiological status (data not shown) and, due to its rare appearance, could not be characterized in detail. At these sites, tonic seizures were variably detected either as a high-frequency activity with or without DC potential shift either in a positive or negative direction.

Together these subcortical recordings demonstrate DC-potential shifts in the SD susceptible striatum and thalamus, while they are rare in the hippocampus and dorsal pons. DC potential shifts in these subcortical regions never preceded a cortical event, and therefore represent either secondary invasion of a cortical SD or independent locally generated depolarization.

I_{NaP} contributes to SD threshold *ex vivo*

We next examined the effect of *Scn8a* GOF mutation on intrinsic tissue SD susceptibility using acute cortical slices prepared from adult *Scn8a*$^{D/+}$ and littermate WT mice. SD susceptibility was measured based on the step-wise incremental elevation of bath $[KCl]_o$, and in this method, the KCl concentration triggering an SD is used as a threshold (**Figure 6A**, see Methods). This assay detected a small decrease in the KCl threshold in *Scn8a*$^{D/+}$ cortical tissue (**Figure 6B**).

The similarity of the cortical bilateral EEG phenotype seen in *Scn8a*$^{D/+}$ and I_{KM} deficient *Kcnq2*-cKO mice raises the possibility that non-inactivating I_{NaP} could directly contribute to the enhanced SD susceptibility. Previous studies report SD inhibition by pan-VGSC inhibitors such as TTX[27–30], however, the specific role of I_{NaP} is not well known. Thus, we analyzed the effect of the I_{NaP} inhibitors Riluzole and GS967[31] on the SD threshold using the same *ex vivo* SD model.

We first examined the effect of TTX, which non-selectively blocks voltage-gated Na^+ currents (VGSC). The addition of 1 μM TTX to the bath solution robustly increased the KCl threshold for triggering SD (**Figure 6C**), validating the contribution of VGSC in SD generation in this assay system.

We then tested the effect of I_{NaP} inhibitors. Riluzole inhibits I_{NaP} with an IC_{50} in the 2-4 μM range[32,33]. We used Riluzole at 5 and 10 μM, which has been shown to inhibit 75-95% of I_{NaP}[32] and 10-20% of glutamate release evoked by high extracellular K^+ [34]. Riluzole at both concentrations increased the KCl threshold for SD in both WT and *Scn8a*$^{D/+}$ cortical slices (**Figure 6D**). A second potent I_{NaP} inhibitor, GS967 at 3 μM, a dosage that preferentially inhibits I_{NaP} over transient Na^+ current[31], also increased KCl threshold for SD in both WT and *Scn8a*$^{D/+}$ cortical tissue (**Figure 6E**). In this comparison, a *Scn8a* genotype difference was not detected because of insufficient statistical power to detect the small mutation effect.

These results demonstrate that I_{NaP}, independent of transient Na^+ current, can influence SD susceptibility *ex vivo*. The more potent SD inhibitory effect of TTX suggests that neuronal firing activity mediated by transient Na^+ currents likely plays an additional downstream effect of I_{NaP} during the initiation of SD (see Discussion).

I_{KM} regulates the *Scn8a*$^{D/+}$ GOF mediated excitabilities

The appearance of SD closely associated with seizure activity in ambulatory mice suggests that SD is generated as a result of hyperexcitable cortical activity. To assess this relationship, we performed *ex vivo* Ca^{2+} imaging using acute horizontal brain slices obtained from *Scn8a*$^{D/+}$ and WT mice carrying a Thy1-GCAMP6s transgene in which a Ca^{2+} sensor GCAMP6s is widely expressed in various brain regions.[18] Our low-magnification fluorescence imaging detected basal Ca^{2+} signals in somatosensory and entorhinal cortices as well as in the hippocampus, and exposure to Mg^{2+}-free bath solution resulted in the generation of large spontaneous fast Ca^{2+} spikes during seizure-like field potentials as well as SD detected as a slowly migrating Ca^{2+} wave (**Figure 7B**).[19,35] While such Ca^{2+} signals were occasionally detected in the striatum and thalamus, they were not reproducible and not analyzed here.

In the somatosensory cortex, the number of SD events generated was higher in *Scn8a*$^{D/+}$ than in the WT cortical slices (**Figure 7C**), demonstrating the higher tissue SD susceptibility in *Scn8a*$^{D/+}$ cortical tissue. In contrast, the number of spikes was not different between genotypes (**Figure 7D**), and bath application of the M-current inhibitor XE991 (10 μM) did not influence the SD or spike frequency in the cortex (**Figure 7C&D)**. In the hippocampus, SD was most consistently detected in the CA3 region and often remained confined within this subfield in both *Scn8a*$^{D/+}$ and WT slices, therefore analysis focused on the CA3 subfield. Neither *Scn8a* genotypes nor XE911 affected the frequency of hippocampal SDs (**Figure 7E**). Unlike the cortex, Ca^{2+} spikes in the CA3 were less frequent in the control condition, however, I_{KM} inhibition by XE991 greatly enhanced them in *Scn8a*$^{D/+}$, but not in the WT slices (**Figure 7F**), suggesting that basal I_{KM} activity restrains *Scn8a* GOF hyperexcitability in this circuit.

In a separate cohort, we examined the effects of the I_{KM} activator ICA-110381, which preferentially potentiates I_{KM} mediated by Kcnq2/3 containing channels with an EC_{50} = 0.38 μM.[36]

These experiments detected fewer Ca^{2+} activities than the experiment above and since SD and spikes in the CA3 were absent in most slices, analysis was focused on cortical events. ICA-110381 at 3 μM eliminated cortical SD (**Figure 7G**) and greatly reduced the number of Ca^{2+} spikes in both WT and *Scn8a*$^{D/+}$ tissue (**Figure 7H**). These results demonstrate that I_{KM} enhancement effectively suppresses cortical hyperexcitability and suggest that the absence of effects seen in the cortical tissue (**Figure 7C&D**) likely reflects the low basal I_{KM}.

Together, these results demonstrate a higher SD susceptibility in the *Scn8a*$^{D/+}$ cortex under hyperexcitable conditions. In addition, the robust increase in hippocampal spiking in the *Scn8a*$^{D/+}$ hippocampal tissue indicates that I_{KM} activity counteracts the *Scn8a*$^{D/+}$ GOF mutation effect.

Discussion

The present study characterized the spatiotemporal seizure-SD phenotype of *Scn8a*$^{D/+}$ mice, revealing a bihemispheric seizure-SD complex as a signature cortical EEG abnormality in this sodium channel GOF mouse model. The LSCI imaging and subcortical EEG recordings studies suggest that the seizure-SD complexes are spontaneously generated in the somatosensory or ventral cortex, and about half of the depolarizing waves spread into the striatum and thalamus, and rarely into hippocampus and brainstem. The similar cortical bilateral seizure-SD phenotype seen in *Kcnq2*-cKO mice suggests that these shared phenotypes can be attributed to an imbalance in the persistent cation currents (I_{NaP}, I_{KM}). Our results collectively indicate that these specific excitability defects can significantly modulate initiation of the self-propagating wave of slow depolarization and suggest that pharmacologically targeting these cation currents might be useful for controlling the SD threshold in epileptic brains.

Regulation of SD threshold by persistent Na^+ and M-type K^+ currents

The present study identifies *Scn8a* as an SD modifier gene. Given the effect of the N1864D mutation on the late sodium channel inactivation, as well as the SD inhibition by I_{NaP} blockers, our study suggests that I_{NaP} is a significant component contributing to SD susceptibility. SD inhibition by the I_{NaP} inhibitor riluzole and GS967 is consistent with their effectiveness at normalizing the

Scn8a GOF effect on neuronal defect in the early afterdepolarization,[37] seizures, and premature death in *Scn8a*$^{D/+}$ mice,[38] as well as reducing seizures in *SCN8A* GOF patients.[39] Our findings are also in line with a previous study reporting that veratridine, a VGSC opener that functionally mimics the *Scn8a*$^{D/+}$ mutation effect,[40] induces seizure-SD complexes in acute hippocampal slices, and I_{NaP} inhibitors reduce them.[41]

The shared bilateral cortical SD phenotype seen in *Scn8a*-GOF and Emx-*Kcnq2* cKO mouse models likely reflects the mutually antagonizing effect of I_{NaP} and I_{KM}. Both I_{NaP} and I_{KM} have slow inactivation kinetics and are activated near the resting membrane potential (~-65 mV).[42,43] Previous studies demonstrated their functional interaction as inhibition of I_{KM} results in the I_{NaP}-mediated burst discharges[44–47] or a plateau depolarization when extracellular Ca^{2+} is reduced.[48,49] The latter might be particularly relevant to the slow ramp membrane depolarization during SD which involves a rapid drop of extracellular Ca^{2+}.[1]

On the other hand, since *Scn8a* and *Kcnq2* are expressed differentially across cell types and brain regions, mutations in these genes will impair the I_{NaP} and I_{KM} balance differently across the brain regions. For example, *Scn8a*$^{D/+}$ mutation increases the excitability of hippocampal pyramidal neurons in both CA1 and CA3 regions, whereas it selectively enhances interneuron excitability in CA3, but not in CA1.[37] A recent study reported that *Kcnq2* GOF mutations increase the excitability of cortical pyramidal neurons but dampen the excitability of hippocampal pyramidal neurons.[50] Similarly, I_{KM} mediated is critical for the medium afterhyperpolarization in CA1 pyramidal neurons,[44,51] but SK-type current may play a larger role in cortical pyramidal and other cell types[52–54]. Such cell type-specific effect could have contributed to the complex sensitivity to the I_{KM} inhibitor XE991 in our *ex vivo* studies (**Figure 7**).

In addition to excitatory neurons, a recent study suggests that increased I_{NaP} in inhibitory neurons due to a *SCN1A* gene mutation identified in familial hemiplegic migraine type 3 (FHM3)[55] can contribute to SD susceptibility.[56] This interneuronal mechanism might also contribute to SD susceptibility in the *Scn8a*$^{D/+}$ mice, especially in the CA3 circuit where the GOF mutation enhances I_{NaP} in interneurons.[37]

Both Nav1.6/*Scn8a* and Kv7.2/*Kcnq2* are highly enriched at the AIS. Correlatively, this compartment has a lower activation threshold for I_{NaP}[57] compared to the soma[46,58] and dendrites,[59,60] and I_{KM} density is higher at the AIS than in the soma.[61,62] Thus, the AIS is likely a

vulnerable region to I_{NaP}/I_{KM} imbalance due to genetic mutation, and a hyperexcitable AIS may contribute to SD susceptibility by increasing action potential frequency.

In addition to AIS, I_{NaP} and I_{KM} coexist in other subcellular compartments relevant to SD. One is the axonal terminal boutons where Nav1.6/*Scn8a*[63] and *Kcnq* channels are detected in some synapses[64–67] and regulate transmitter release. In fact, inhibition of Na^+ current at the release site was considered as a mechanism by which the I_{NaP} inhibitor riluzole inhibits glutamate release.[34]

Studies also suggest I_{NaP} and I_{KM} could modify postsynaptic currents. Immuno-electron microscopy studies have detected Nav1.6/*Scn8a*[63] and Kv7.2/*Kcnq2*[68] in dendritic spines. In support of a postsynaptic role of I_{KM}, several I_{KM} activators act as functional NMDAR antagonists, likely by stabilizing the Mg^{2+} channel block,[69,70] which would contribute to their SD inhibitory effect.[17,71] While the physiological significance, molecular composition, and cell/species-specificity are not fully understood, postsynaptic I_{NaP}/I_{KM} dysfunction may influence SD susceptibility.

SD and tonic seizures

Profound tonic spastic seizure without or minimum clonus is a robust clinical phenotype in *Scn8a*$^{D/+}$ mice. *Scn8a* is expressed in murine spinal motoneurons,[72] and the GOF mutation may directly increase the susceptibility to neurogenic spasms.[73] The frequent appearance of tonic spasms during and after seizure-SD complex suggests that SD might create an excitatory brain state favoring this paroxysmal motor event. On the other hand, unlike previous studies,[74] SD was absent when tonic spasm was provoked as audiogenic seizure, indicating that SD is not required for the onset.

In addition to their spontaneous appearance, recurrent tonic seizures could be reproduced during bilateral SD in *Scn8a*$^{D/+}$ mice injected with PTZ (**Figure 4**). These tonic seizures were associated with abrupt apnea as reported previously[75] as well as a rapid global CBF decrease and massive salivation (**Figure 4**). We speculate these responses reflect systemic parasympathetic overactivation which could reduce cerebral perfusion pressure and enhance salivation. SD was always followed by an hour-lasting period of hypoperfusion, which was previously detected with a laser-doppler system during KCl-induced SD,[76] and a similar prolonged hypoperfusion occurrs

after a hippocampal seizure.[77] These hour-lasting hypoperfusion are mediated by COX1/2 metabolites,[77–79] and the response seen in our model likely share the underlying molecular mechanism.

Tonic seizures are also a prominent clinical feature of *KCNQ2*-associated developmental encephalopathy patients,[80,81] suggesting a pathophysiological similarity to *SCN8A* encephalopathy. However, our previous studies on mice with forebrain-specific *Kcnq2* deletion (Emx1-*Kcnq2* cKO) did not detect robust tonic seizures as seen in *Scn8a*$^{D/+}$ mice. This might reflect localization of the *Kcnq2*-sensitive spastic mechanism outside the forebrain such as in the extrapyramidal pathways[82] and/or spinal motoneurons,[83,84] or the *KCNQ2*-related clinical phenotype is not fully recapitulated in the mouse. On the other hand, the extremely high premature mortality (>90% before P30) in Emx1-*Kcnq2* cKO mice[85] is not seen in *Scn8a*$^{D/+}$ mice, and thus downstream pathways affecting the seizure-induced death, such as peripheral autonomic ganglia,[86] might be less affected in *Scn8a*$^{D/+}$ mice.

SD and seizures in subcortical structures

Our subcortical recordings revealed extensive depolarization of deep brain regions associated with cortical seizure-SD complexes. In the striatum, cortical SD was followed by delayed depolarization. A previous study suggested this is the invasion of cortical wave spreading through the piriform/amygdala complex.[87] If the propagation pattern is shared, SD invasion into these ventral cortical areas may contribute to autonomic dysfunction in *Scn8a*$^{D/}$+ mice.

We detected SD-like DC potential shifts in the thalamus. A thalamic SD has been reported in a *Canca1a* GOF model[23] and was accompanied by transient hypertension. The thalamic DC potential shift detected in the *Scn8a*$^{D/+}$ mice closely coincided with cortical depolarization and was therefore unlikely to represent an invasion of the cortical wave. Rather, the near-simultaneous cortico-thalamic depolarization suggests it is related to the putative synaptic activation of the thalamic neurons during cortical SD wave reported in awake mice.[88]

SD incidence was rare in the hippocampus. This result was somewhat unexpected because hippocampus, especially CA1, is relatively SD-susceptible,[1] and the excitability of pyramidal neurons in the hippocampus and adjacent entorhinal cortex is increased in *Scn8a*$^{D/+}$ mice.[37,89] SD

threshold in the hippocampus might be less sensitive to I_{NaP}/I_{KM} imbalance or, alternatively, this could be related to SD resistance reported in highly epileptic tissue.[90] On the other hand, we cannot exclude the possibility that our single channel recording with a fine wire electrode could have missed a localized SD event as was seen in our *ex vivo* Ca^{2+} imaging study.

The inferior colliculus and pontine nucleus rarely show SD events, which is consistent with their low SD susceptibility and the *Scn8a*$^{D/+}$ mutation alone did not overcome the high SD threshold. However, SD susceptibility in these brainstem structures might be increased in younger animals with low myelination and a higher vulnerability to abnormal excitation as suggested by their higher susceptibility to audiogenic seizures. These brainstem structures also lacked ictal discharges during cortical seizure, yet displayed clear activity associated with tonic seizures, suggesting brainstem circuits at this level are involved in the paroxysmal spastic pathology. Fine mapping of the brainstem circuit involved in tonic seizure would facilitate the development of therapeutics relevant to brainstem hyperexcitability associated with *SCN8A* and *KCNQ2* mutations.

In summary, the present study identified a shared susceptibility to bilateral SD wave in *Scn8a* GOF and *Kcnq2*-cKO mice, which suggests a putative role of I_{NaP} and I_{KM} balance in the regulation of SD generation and propagation. The frequent interaction between seizure and SD seen in these DEE models suggests SD might be involved in the spectrum of comorbidities in patients associated with these ion channelopathies.

Funding

NINDS NS29709 (JLN), Blue Bird Circle (JLN), AES junior investigator award (IA)

Competing interests

None

References

1 Somjen GG. Mechanisms of spreading depression and hypoxic spreading depression-like depolarization. *Physiol Rev* 2001;**81**:1065–96. https://doi.org/10.1152/physrev.2001.81.3.1065.

2 Dreier JP. The role of spreading depression, spreading depolarization and spreading ischemia in neurological disease. *Nat Med* 2011;**17**:439–47. https://doi.org/10.1038/nm.2333.

3 Weckhuysen S, Mandelstam S, Suls A, Audenaert D, Deconinck T, Claes LRF, *et al. KCNQ2* encephalopathy: Emerging phenotype of a neonatal epileptic encephalopathy. *Annals of Neurology* 2012;**71**:15–25. https://doi.org/10.1002/ana.22644.

4 Berg AT, Mahida S, Poduri A. *KCNQ2* -DEE: developmental or epileptic encephalopathy? *Ann Clin Transl Neurol* 2021;**8**:666–76. https://doi.org/10.1002/acn3.51316.

5 Aiba I, Noebels JL. Kcnq2/Kv7.2 controls the threshold and bihemispheric symmetry of cortical spreading depolarization. *Brain* 2021;**144**:2863–78. https://doi.org/10.1093/brain/awab141.

6 Pan Z, Kao T, Horvath Z, Lemos J, Sul J-Y, Cranstoun SD, *et al.* A common ankyrin-G-based mechanism retains KCNQ and NaV channels at electrically active domains of the axon. *J Neurosci* 2006;**26**:2599–613. https://doi.org/10.1523/JNEUROSCI.4314-05.2006.

7 Klinger F, Gould G, Boehm S, Shapiro MS. Distribution of M-channel subunits KCNQ2 and KCNQ3 in rat hippocampus. *NeuroImage* 2011;**58**:761–9. https://doi.org/10.1016/j.neuroimage.2011.07.003.

8 Huang CY-M, Rasband MN. Axon initial segments: structure, function, and disease. *Ann N Y Acad Sci* 2018;**1420**:46–61. https://doi.org/10.1111/nyas.13718.

9 Lorincz A, Nusser Z. Cell-type-dependent molecular composition of the axon initial segment. *J Neurosci* 2008;**28**:14329–40. https://doi.org/10.1523/JNEUROSCI.4833-08.2008.

10 Rush AM, Dib-Hajj SD, Waxman SG. Electrophysiological properties of two axonal sodium channels, Nav1.2 and Nav1.6, expressed in mouse spinal sensory neurones. *J Physiol* 2005;**564**:803–15. https://doi.org/10.1113/jphysiol.2005.083089.

11 Zhou W, Goldin AL. Use-dependent potentiation of the Nav1.6 sodium channel. *Biophys J* 2004;**87**:3862–72. https://doi.org/10.1529/biophysj.104.045963.

12 Chen Y, Yu FH, Sharp EM, Beacham D, Scheuer T, Catterall WA. Functional properties and differential neuromodulation of Na(v)1.6 channels. *Mol Cell Neurosci* 2008;**38**:607–15. https://doi.org/10.1016/j.mcn.2008.05.009.

13 Veeramah KR, O'Brien JE, Meisler MH, Cheng X, Dib-Hajj SD, Waxman SG, *et al.* De novo pathogenic SCN8A mutation identified by whole-genome sequencing of a family quartet affected by infantile epileptic encephalopathy and SUDEP. *Am J Hum Genet* 2012;**90**:502–10. https://doi.org/10.1016/j.ajhg.2012.01.006.

14 Talwar D, Hammer MF. SCN8A Epilepsy, Developmental Encephalopathy, and Related Disorders. *Pediatric Neurology* 2021;**122**:76–83. https://doi.org/10.1016/j.pediatrneurol.2021.06.011.

15 Wagnon JL, Korn MJ, Parent R, Tarpey TA, Jones JM, Hammer MF, *et al.* Convulsive seizures and SUDEP in a mouse model of SCN8A epileptic encephalopathy. *Hum Mol Genet* 2015;**24**:506–15. https://doi.org/10.1093/hmg/ddu470.

16 Ottolini M, Barker BS, Gaykema RP, Meisler MH, Patel MK. Aberrant Sodium Channel Currents and Hyperexcitability of Medial Entorhinal Cortex Neurons in a Mouse Model of SCN8A Encephalopathy. *J Neurosci* 2017;**37**:7643–55. https://doi.org/10.1523/JNEUROSCI.2709-16.2017.

17 Aiba I, Noebels JL. *Kcnq2/Kv7.2 controls the threshold and bihemispheric symmetry of cortical spreading depolarization*. Neuroscience; 2020.

18 Dana H, Chen T-W, Hu A, Shields BC, Guo C, Looger LL, *et al.* Thy1-GCaMP6 transgenic mice for neuronal population imaging in vivo. *PLoS One* 2014;**9**:e108697. https://doi.org/10.1371/journal.pone.0108697.

19 Aiba I, Wehrens XHT, Noebels JL. Leaky RyR2 channels unleash a brainstem spreading depolarization mechanism of sudden cardiac death. *Proc Natl Acad Sci USA* 2016;**113**:E4895-4903. https://doi.org/10.1073/pnas.1605216113.

20 Dunn AK. Laser speckle contrast imaging of cerebral blood flow. *Ann Biomed Eng* 2012;**40**:367–77. https://doi.org/10.1007/s10439-011-0469-0.

21 Koroleva VI, Vinogradova LV, Bures J. Reduced incidence of cortical spreading depression in the course of pentylenetetrazol kindling in rats. *Brain Res* 1993;**608**:107–14. https://doi.org/10.1016/0006-8993(93)90780-q.

22 Sosulski DL, Bloom ML, Cutforth T, Axel R, Datta SR. Distinct representations of olfactory information in different cortical centres. *Nature* 2011;**472**:213–6. https://doi.org/10.1038/nature09868.

23 Eikermann-Haerter K, Yuzawa I, Qin T, Wang Y, Baek K, Kim YR, *et al.* Enhanced subcortical spreading depression in familial hemiplegic migraine type 1 mutant mice. *J Neurosci* 2011;**31**:5755–63. https://doi.org/10.1523/JNEUROSCI.5346-10.2011.

24 Jansen NA, Schenke M, Voskuyl RA, Thijs RD, van den Maagdenberg AMJM, Tolner EA. Apnea Associated with Brainstem Seizures in Cacna1aS218L Mice Is Caused by Medullary Spreading Depolarization. *J Neurosci* 2019;**39**:9633–44. https://doi.org/10.1523/JNEUROSCI.1713-19.2019.

25 Loonen ICM, Voskuyl RA, Schenke M, Van Heiningen SH, Van Den Maagdenberg AMJM, Tolner EA. Spontaneous and optogenetically induced cortical spreading depolarization in familial hemiplegic migraine type 1 mutant mice. *Neurobiology of Disease* 2024;**192**:106405. https://doi.org/10.1016/j.nbd.2024.106405.

26 Vinogradova LV, Koroleva VI, Bures J. Re-entry waves of Leao's spreading depression between neocortex and caudate nucleus. *Brain Res* 1991;**538**:161–4. https://doi.org/10.1016/0006-8993(91)90392-9.

27 Müller M, Somjen GG. Na(+) and K(+) concentrations, extra- and intracellular voltages, and the effect of TTX in hypoxic rat hippocampal slices. *J Neurophysiol* 2000;**83**:735–45. https://doi.org/10.1152/jn.2000.83.2.735.

28 Aitken PG, Tombaugh GC, Turner DA, Somjen GG. Similar propagation of SD and hypoxic SD-like depolarization in rat hippocampus recorded optically and electrically. *J Neurophysiol* 1998;**80**:1514–21. https://doi.org/10.1152/jn.1998.80.3.1514.

29 Xie Y, Dengler K, Zacharias E, Wilffert B, Tegtmeier F. Effects of the sodium channel blocker tetrodotoxin (TTX) on cellular ion homeostasis in rat brain subjected to complete ischemia. *Brain Res* 1994;**652**:216–24. https://doi.org/10.1016/0006-8993(94)90230-5.

30 Suryavanshi P, Reinhart KM, Shuttleworth CW, Brennan KC. Action Potentials Are Critical for the Propagation of Focally Elicited Spreading Depolarizations. *J Neurosci* 2022;**42**:2371–83. https://doi.org/10.1523/JNEUROSCI.2930-20.2021.

31 Müller P, Draguhn A, Egorov AV. Persistent sodium currents in neurons: potential mechanisms and pharmacological blockers. *Pflugers Arch - Eur J Physiol* 2024. https://doi.org/10.1007/s00424-024-02980-7.

32 Urbani A, Belluzzi O. Riluzole inhibits the persistent sodium current in mammalian CNS neurons. *Eur J of Neuroscience* 2000;**12**:3567–74. https://doi.org/10.1046/j.1460-9568.2000.00242.x.

33 Xie R-G, Zheng D-W, Xing J-L, Zhang X-J, Song Y, Xie Y-B, *et al.* Blockade of persistent sodium currents contributes to the riluzole-induced inhibition of spontaneous activity and oscillations in injured DRG neurons. *PLoS One* 2011;**6**:e18681. https://doi.org/10.1371/journal.pone.0018681.

34 Martin D, Thompson MA, Nadler JV. The neuroprotective agent riluzole inhibits release of glutamate and aspartate from slices of hippocampal area CA1. *Eur J Pharmacol* 1993;**250**:473–6. https://doi.org/10.1016/0014-2999(93)90037-i.

35 Mody I, Lambert JD, Heinemann U. Low extracellular magnesium induces epileptiform activity and spreading depression in rat hippocampal slices. *J Neurophysiol* 1987;**57**:869–88. https://doi.org/10.1152/jn.1987.57.3.869.

36 Boehlen A, Schwake M, Dost R, Kunert A, Fidzinski P, Heinemann U, *et al.* The new KCNQ2 activator 4-Chlor-N-(6-chlor-pyridin-3-yl)-benzamid displays anticonvulsant potential. *Br J Pharmacol* 2013;**168**:1182–200. https://doi.org/10.1111/bph.12065.

37 Lopez-Santiago LF, Yuan Y, Wagnon JL, Hull JM, Frasier CR, O'Malley HA, *et al.* Neuronal hyperexcitability in a mouse model of SCN8A epileptic encephalopathy. *Proc Natl Acad Sci U S A* 2017;**114**:2383–8. https://doi.org/10.1073/pnas.1616821114.

38 Baker EM, Thompson CH, Hawkins NA, Wagnon JL, Wengert ER, Patel MK, *et al.* The novel sodium channel modulator GS-458967 (GS967) is an effective treatment in a mouse model of SCN8A encephalopathy. *Epilepsia* 2018;**59**:1166–76. https://doi.org/10.1111/epi.14196.

39 Tidball AM, Lopez-Santiago LF, Yuan Y, Glenn TW, Margolis JL, Clayton Walker J, *et al.* Variant-specific changes in persistent or resurgent sodium current in SCN8A-related epilepsy patient-derived neurons. *Brain* 2020;**143**:3025–40. https://doi.org/10.1093/brain/awaa247.

40 Zhu H-L, Wassall RD, Takai M, Morinaga H, Nomura M, Cunnane TC, *et al.* Actions of veratridine on tetrodotoxin-sensitive voltage-gated Na currents, Na1.6, in murine vas deferens

myocytes. *Br J Pharmacol* 2009;**157**:1483–93. https://doi.org/10.1111/j.1476-5381.2009.00301.x.

41 Ashton D, Willems R, Wynants J, Van Reempts J, Marrannes R, Clincke G. Altered Na(+)-channel function as an in vitro model of the ischemic penumbra: action of lubeluzole and other neuroprotective drugs. *Brain Res* 1997;**745**:210–21. https://doi.org/10.1016/s0006-8993(96)01094-3.

42 French CR, Sah P, Buckett KJ, Gage PW. A voltage-dependent persistent sodium current in mammalian hippocampal neurons. *J Gen Physiol* 1990;**95**:1139–57. https://doi.org/10.1085/jgp.95.6.1139.

43 Halliwell JV, Adams PR. Voltage-clamp analysis of muscarinic excitation in hippocampal neurons. *Brain Res* 1982;**250**:71–92. https://doi.org/10.1016/0006-8993(82)90954-4.

44 Yue C, Yaari Y. KCNQ/M channels control spike afterdepolarization and burst generation in hippocampal neurons. *J Neurosci* 2004;**24**:4614–24. https://doi.org/10.1523/JNEUROSCI.0765-04.2004.

45 Gu N, Vervaeke K, Hu H, Storm JF. Kv7/KCNQ/M and HCN/h, but not KCa2/SK channels, contribute to the somatic medium after-hyperpolarization and excitability control in CA1 hippocampal pyramidal cells. *J Physiol* 2005;**566**:689–715. https://doi.org/10.1113/jphysiol.2005.086835.

46 Yue C, Remy S, Su H, Beck H, Yaari Y. Proximal persistent Na+ channels drive spike afterdepolarizations and associated bursting in adult CA1 pyramidal cells. *J Neurosci* 2005;**25**:9704–20. https://doi.org/10.1523/JNEUROSCI.1621-05.2005.

47 Verneuil J, Brocard C, Trouplin V, Villard L, Peyronnet-Roux J, Brocard F. The M-current works in tandem with the persistent sodium current to set the speed of locomotion. *PLoS Biol* 2020;**18**:e3000738. https://doi.org/10.1371/journal.pbio.3000738.

48 Caspi A, Benninger F, Yaari Y. KV7/M channels mediate osmotic modulation of intrinsic neuronal excitability. *J Neurosci* 2009;**29**:11098–111. https://doi.org/10.1523/JNEUROSCI.0942-09.2009.

49 Golomb D, Yue C, Yaari Y. Contribution of persistent Na+ current and M-type K+ current to somatic bursting in CA1 pyramidal cells: combined experimental and modeling study. *J Neurophysiol* 2006;**96**:1912–26. https://doi.org/10.1152/jn.00205.2006.

50 Varghese N, Moscoso B, Chavez A, Springer K, Ortiz E, Soh H, *et al.* KCNQ2/3 Gain-of-Function Variants and Cell Excitability: Differential Effects in CA1 versus L2/3 Pyramidal Neurons. *J Neurosci* 2023;**43**:6479–94. https://doi.org/10.1523/JNEUROSCI.0980-23.2023.

51 Storm JF. Action potential repolarization and a fast after-hyperpolarization in rat hippocampal pyramidal cells. *J Physiol* 1987;**385**:733–59. https://doi.org/10.1113/jphysiol.1987.sp016517.

52 Gu N, Hu H, Vervaeke K, Storm JF. SK (KCa2) channels do not control somatic excitability in CA1 pyramidal neurons but can be activated by dendritic excitatory synapses and regulate their impact. *J Neurophysiol* 2008;**100**:2589–604. https://doi.org/10.1152/jn.90433.2008.

53 Villalobos C, Shakkottai VG, Chandy KG, Michelhaugh SK, Andrade R. SKCa channels mediate the medium but not the slow calcium-activated afterhyperpolarization in cortical neurons. *J Neurosci* 2004;**24**:3537–42. https://doi.org/10.1523/JNEUROSCI.0380-04.2004.

54 Ikeda K, Suzuki N, Bekkers JM. Sodium and potassium conductances in principal neurons of the mouse piriform cortex: a quantitative description. *J Physiol* 2018;**596**:5397–414. https://doi.org/10.1113/JP275824.

55 Brunklaus A, Brünger T, Feng T, Fons C, Lehikoinen A, Panagiotakaki E, *et al.* The gain of function SCN1A disorder spectrum: novel epilepsy phenotypes and therapeutic implications. *Brain* 2022;**145**:3816–31. https://doi.org/10.1093/brain/awac210.

56 Chever O, Zerimech S, Scalmani P, Lemaire L, Pizzamiglio L, Loucif A, *et al.* Initiation of migraine-related cortical spreading depolarization by hyperactivity of GABAergic neurons and NaV1.1 channels. *J Clin Invest* 2021;**131**:e142203. https://doi.org/10.1172/JCI142203.

57 Shvartsman A, Kotler O, Stoler O, Khrapunsky Y, Melamed I, Fleidervish IA. Subcellular distribution of persistent sodium conductance in cortical pyramidal neurons. *J Neurosci* 2021;**41**:6190–201. https://doi.org/10.1523/JNEUROSCI.2989-20.2021.

58 Andreasen M, Lambert JD. Somatic amplification of distally generated subthreshold EPSPs in rat hippocampal pyramidal neurones. *J Physiol* 1999;**519 Pt 1**:85–100. https://doi.org/10.1111/j.1469-7793.1999.0085o.x.

59 Hsu C-L, Zhao X, Milstein AD, Spruston N. Persistent Sodium Current Mediates the Steep Voltage Dependence of Spatial Coding in Hippocampal Pyramidal Neurons. *Neuron* 2018;**99**:147-162.e8. https://doi.org/10.1016/j.neuron.2018.05.025.

60 Lipowsky R, Gillessen T, Alzheimer C. Dendritic Na+ channels amplify EPSPs in hippocampal CA1 pyramidal cells. *J Neurophysiol* 1996;**76**:2181–91. https://doi.org/10.1152/jn.1996.76.4.2181.

61 Battefeld A, Tran BT, Gavrilis J, Cooper EC, Kole MHP. Heteromeric Kv7.2/7.3 channels differentially regulate action potential initiation and conduction in neocortical myelinated axons. *J Neurosci* 2014;**34**:3719–32. https://doi.org/10.1523/JNEUROSCI.4206-13.2014.

62 Hu W, Bean BP. Differential Control of Axonal and Somatic Resting Potential by Voltage-Dependent Conductances in Cortical Layer 5 Pyramidal Neurons. *Neuron* 2018;**97**:1315-1326.e3. https://doi.org/10.1016/j.neuron.2018.02.016.

63 Johnson KW, Herold KF, Milner TA, Hemmings HC, Platholi J. Sodium channel subtypes are differentially localized to pre- and post-synaptic sites in rat hippocampus. *J of Comparative Neurology* 2017;**525**:3563–78. https://doi.org/10.1002/cne.24291.

64 Engel D, Jonas P. Presynaptic Action Potential Amplification by Voltage-Gated Na+ Channels in Hippocampal Mossy Fiber Boutons. *Neuron* 2005;**45**:405–17. https://doi.org/10.1016/j.neuron.2004.12.048.

65 Martinello K, Giacalone E, Migliore M, Brown DA, Shah MM. The subthreshold-active KV7 current regulates neurotransmission by limiting spike-induced Ca2+ influx in hippocampal mossy fiber synaptic terminals. *Commun Biol* 2019;**2**:145. https://doi.org/10.1038/s42003-019-0408-4.

66 Huang H, Trussell LO. Control of presynaptic function by a persistent Na(+) current. *Neuron* 2008;**60**:975–9. https://doi.org/10.1016/j.neuron.2008.10.052.

67 Huang H, Trussell LO. KCNQ5 channels control resting properties and release probability of a synapse. *Nat Neurosci* 2011;**14**:840–7. https://doi.org/10.1038/nn.2830.

68 Galvin VC, Yang ST, Paspalas CD, Yang Y, Jin LE, Datta D, *et al.* Muscarinic M1 Receptors Modulate Working Memory Performance and Activity via KCNQ Potassium Channels in the Primate Prefrontal Cortex. *Neuron* 2020;**106**:649-661.e4. https://doi.org/10.1016/j.neuron.2020.02.030.

69 Kornhuber J, Bleich S, Wiltfang J, Maler M, Parsons CG. Flupirtine shows functional NMDA receptor antagonism by enhancing Mg 2+ block via activation of voltage independent potassium channels. *Journal of Neural Transmission* 1999;**106**:857–67. https://doi.org/10.1007/s007020050206.

70 Jaeger HM, Pehlke JR, Kaltwasser B, Kilic E, Bähr M, Hermann DM, *et al.* The indirect NMDAR inhibitor flupirtine induces sustained post-ischemic recovery, neuroprotection and angioneurogenesis. *Oncotarget* 2015;**6**:14033–44. https://doi.org/10.18632/oncotarget.4226.

71 Wu Y-J, Boissard CG, Greco C, Gribkoff VK, Harden DG, He H, *et al.* (S)-N-[1-(3-morpholin-4-ylphenyl)ethyl]- 3-phenylacrylamide: an orally bioavailable KCNQ2 opener with significant activity in a cortical spreading depression model of migraine. *J Med Chem* 2003;**46**:3197–200. https://doi.org/10.1021/jm034073f.

72 Drouillas B, Brocard C, Zanella S, Bos R, Brocard F. Persistent Nav1.1 and Nav1.6 currents drive spinal locomotor functions through nonlinear dynamics. *Cell Rep* 2023;**42**:113085. https://doi.org/10.1016/j.celrep.2023.113085.

73 Gorassini MA, Knash ME, Harvey PJ, Bennett DJ, Yang JF. Role of motoneurons in the generation of muscle spasms after spinal cord injury. *Brain* 2004;**127**:2247–58. https://doi.org/10.1093/brain/awh243.

74 Vinogradova LV, Kuznetsova GD, Coenen AML. Unilateral cortical spreading depression induced by sound in rats. *Brain Research* 2009;**1286**:201–7. https://doi.org/10.1016/j.brainres.2009.06.047.

75 Wenker IC, Teran FA, Wengert ER, Wagley PK, Panchal PS, Blizzard EA, *et al.* Postictal Death Is Associated with Tonic Phase Apnea in a Mouse Model of Sudden Unexpected Death in Epilepsy. *Ann Neurol* 2021;**89**:1023–35. https://doi.org/10.1002/ana.26053.

76 Ayata C, Shin HK, Salomone S, Ozdemir-Gursoy Y, Boas DA, Dunn AK, *et al.* Pronounced hypoperfusion during spreading depression in mouse cortex. *J Cereb Blood Flow Metab* 2004;**24**:1172–82. https://doi.org/10.1097/01.WCB.0000137057.92786.F3.

77 Farrell JS, Gaxiola-Valdez I, Wolff MD, David LS, Dika HI, Geeraert BL, *et al.* Postictal behavioural impairments are due to a severe prolonged hypoperfusion/hypoxia event that is COX-2 dependent. *Elife* 2016;**5**:. https://doi.org/10.7554/eLife.19352.

78 Zhao J, Levy D. Dissociation between CSD-Evoked Metabolic Perturbations and Meningeal Afferent Activation and Sensitization: Implications for Mechanisms of Migraine Headache Onset. *J Neurosci* 2018;**38**:5053–66. https://doi.org/10.1523/JNEUROSCI.0115-18.2018.

79 Gariepy H, Zhao J, Levy D. Differential contribution of COX-1 and COX-2 derived prostanoids to cortical spreading depression-Evoked cerebral oligemia. *J Cereb Blood Flow Metab* 2017;**37**:1060–8. https://doi.org/10.1177/0271678X16650217.

80 Pisano T, Numis AL, Heavin SB, Weckhuysen S, Angriman M, Suls A, *et al.* Early and effective treatment of *KCNQ 2* encephalopathy. *Epilepsia* 2015;**56**:685–91. https://doi.org/10.1111/epi.12984.

81 Gomis-Pérez C, Urrutia J, Marcé-Grau A, Malo C, López-Laso E, Felipe-Rucián A, *et al.* Homomeric Kv7.2 current suppression is a common feature in KCNQ2 epileptic encephalopathy. *Epilepsia* 2019;**60**:139–48. https://doi.org/10.1111/epi.14609.

82 McCall AA, Miller DM, Yates BJ. Descending Influences on Vestibulospinal and Vestibulosympathetic Reflexes. *Front Neurol* 2017;**8**:112. https://doi.org/10.3389/fneur.2017.00112.

83 Sharples SA, Broadhead MJ, Gray JA, Miles GB. M-type potassium currents differentially affect activation of motoneuron subtypes and tune recruitment gain. *J Physiol* 2023;**601**:5751–75. https://doi.org/10.1113/JP285348.

84 Lombardo J, Sun J, Harrington MA. Rapid activity-dependent modulation of the intrinsic excitability through up-regulation of KCNQ/Kv7 channel function in neonatal spinal motoneurons. *PLoS One* 2018;**13**:e0193948. https://doi.org/10.1371/journal.pone.0193948.

85 Soh H, Pant R, LoTurco JJ, Tzingounis AV. Conditional deletions of epilepsy-associated KCNQ2 and KCNQ3 channels from cerebral cortex cause differential effects on neuronal excitability. *J Neurosci* 2014;**34**:5311–21. https://doi.org/10.1523/JNEUROSCI.3919-13.2014.

86 Ning Y, Noebels JL, Aiba I. Emx1-Cre is expressed in peripheral autonomic ganglia that regulate central cardiorespiratory functions. *eNeuro* 2022:ENEURO.0093-22.2022. https://doi.org/10.1523/ENEURO.0093-22.2022.

87 Fifková E, Syka J. Relationships between cortical and striatal spreading depression in rat. *Experimental Neurology* 1964;**9**:355–66. https://doi.org/10.1016/0014-4886(64)90070-6.

88 Fu X, Chen M, Lu J, Li P. Cortical spreading depression induces propagating activation of the thalamus ventral posteromedial nucleus in awake mice. *J Headache Pain* 2022;**23**:15. https://doi.org/10.1186/s10194-021-01370-z.

89 Ottolini M, Barker BS, Gaykema RP, Meisler MH, Patel MK. Aberrant Sodium Channel Currents and Hyperexcitability of Medial Entorhinal Cortex Neurons in a Mouse Model of SCN8A Encephalopathy. *J Neurosci* 2017;**37**:7643–55. https://doi.org/10.1523/JNEUROSCI.2709-16.2017.

90 Maslarova A, Alam M, Reiffurth C, Lapilover E, Gorji A, Dreier JP. Chronically epileptic human and rat neocortex display a similar resistance against spreading depolarization in vitro. *Stroke* 2011;**42**:2917–22. https://doi.org/10.1161/STROKEAHA.111.621581.

Figure legends

Figure 1

Chronic DC-band EEG recording in *Scn8a*$^{D/+}$ mice. **A.** scheme showing four cortical EEG electrode implant positions and example of a ~12-hour EEG trace. **B.** Expanded EEG trace of bilateral seizure-SD complex. **C.** Box-whisker plots showing the frequency of bilateral seizure-SD complexes (left), unilateral seizure-SD complexes (middle), and seizures (right). The values over the plots indicate mean standard ± deviation and median in parentheses. **D.** Raster plot of cortical EEG events across ages. M: male, F: female **F.** Cumulative histograms of detected cortical EEG events by time of day. Dashed lines show a density plot.

Figure 2

Electrographic characterization of cortical seizure-SD complex in *Scn8a*$^{D/+}$ mice. A. Representative DC-band and high-pass filtered (>1Hz) EEG traces and power spectrum of a seizure-SD complex. The expanded EEG traces in orange boxes corresponding to a. ictal and b. tonic seizure are presented in **B&C**. SD onset was preceded by a seizure characterized by a robust tonic seizure detected as high-frequency noise (blue shade), followed by slow ictal spikes (**B**). After an SD, another tonic seizure was detected as high-frequency activity (blue shade) (**C**). Mouse posture associated with tonic seizures is typically characterized by a hunched back and hind limb extension as shown in the right panel. **D.** The number of tonic seizures during a seizure-SD episode. About one-third of events were associated with only one tonic seizure at the SD onset (n=1), while the rest of the seizure-SD episodes were associated with one or two post-SD tonic seizures (n=2 and 3).

Figure 3

Audiogenic seizure did not involve cortical SD. An audiogenic seizure was provoked by a loud buzzer in *Scn8a*$^{D/+}$ mice implanted with cortical EEG electrodes as shown in **Figure 1**. A robust tonic spasm was detected during audiogenic seizure, however, no SD-like DC potential shift was detected in all six recordings.

Figure 4

Combined electrophysiological and laser speckle contrast imaging of head-restrained awake mice injected with PTZ. A. Sequence LSCI images of bilateral SD detected as waves of hypoperfusion (wavefront shown with yellow arrow) advancing symmetrically from the lateral to the midline. The raw contrast value (standard deviation/mean) from the region of interest (ROI) was used as the CBF readout. **B.** Cortical EEG, EMG, nasal airflow, and relative CBF changes during an episode of seizure-SD complex after a single injection of PTZ, and the onset of cortical SD with tonic seizures is expanded in **C**. Tonic seizures (blue shade) were detected as enhanced EMG signal at the onset and during cortical SD. During tonic seizures, nasal airflow was absent and CBF was slightly reduced. **D.** Images of mouse behaviors. During baseline, the mouse is firmly grabbing the running wheel to maintain posture. During tonic seizure, forelimbs are retracted and eyes are partially closed. After the second tonic seizure, massive salivation was detected. After SD, the mouse became immobile and often did not grab the running wheel. **E.** SD waves in *Scn8a*$^{D/+}$ mice were always bilateral, while only 25% of them were bilateral in WT. The amplitudes of the DC potential shift were similar (**F**), while the duration was prolonged in *Scn8a*$^{D/+}$ mice (**G**). **H.** Tonic seizures were only seen in *Scn8a*$^{D/+}$ mice. **I.** The mean trace of normalized CBF changes in WT and *Scn8a*$^{D/+}$ mice from 5 recordings. Shades indicate 95% confidential interval.

Figure 5

Combined cortical surface and subcortical EEG recordings. A. Cortical seizure-SD complex simultaneously recorded in cortical and hippocampal electrodes**.** Seizures were simultaneously detected both in the cortex and hippocampus, however, SD was often absent in the hippocampus. The histology image on the right shows the electrode recording site determined by DiD fluorescence marking the electrode tip. **B.** In striatum recordings, cortical seizure-SD complex was

detected as seizure only, however, a delayed DC potential shift is often detected. **C.** In the thalamus, sharp DC potential shift was often detected in association with DC potential shift in the cortex. Tonic seizures were detected as relatively large DC potential shifts in this region. **D.** Recordings from inferior colliculus and pontine nucleus. In these structures, cortical seizure-like discharge was absent, while delayed activity was detected during cortical SD. SD was rarely detected. In this structure, tonic seizures were detected with variable patterns, either with or without DC potential shift.

Figure 6

***Ex vivo* SD threshold test revealed a contribution of I_{NaP} to the SD threshold.** Slices were incubated in ACSF while KCl concentration was incrementally elevated by 1 mM until SD was generated. **A.** Raw image (left) and ratio images (2^{nd}-4^{th} images). SD wave can be readily detected as an enhanced IOS signal. Arrows mark the leading edge of SD. Scale bar 500 µm. **B.** KCl concentration was slightly lowered in *Scn8a*$^{D/+}$ slices. **C.** TTX increased KCl concentration required to trigger SD. **D.** I_{NaP} inhibitor riluzole increased KCl concentration to trigger SD in WT and *Scn8a*$^{D/+}$ slices. In WT, One-Way ANOVA, p= <0.0001. **E.** A similar inhibitory effect was seen with I_{NaP} inhibitor GS967.

Figure 7

***Ex vivo* Ca^{2+} imaging analysis of the effect of I_{KM} modulators on cortical and hippocampal SD and epileptic activities. A&B** Representative images and traces of tissue excitability test by *ex vivo* Ca^{2+} imaging. Horizontal slices obtained from WT- or *Scn8a*$^{D/+}$-GCAMP6s slices were incubated in Mg^{2+} free ACSF. **A.** Raw and ratio fluorescence images showing Ca^{2+} activities in the cortex and hippocampus CA3. SD was detected as a prolonged Ca^{2+} elevation whereas seizure-like activities were detected as fast Ca^{2+} spikes (**B** inset). **C-F** Effect of I_{KM} inhibitor XE991. **C.** Cortical SD were more frequently generated in the *Scn8a*$^{D/+}$ than WT and XE991 was without effect (genotype: p=0.009, XE991: p>0.57, interaction: p>0.57) **D.** There was no genotype or XE991 effect in the cortical Ca^{2+} spikes (genotype: p>0.41, XE991: p>0.60, interaction: p=0.017). **E.** The SD frequency in the CA3 was not modified by genotype or XE991 treatment. (genotype:

p>0.10, XE991: p>0.99, interaction: p>0.10). **F.** Spike frequency in the CA3 was low in the control condition, but XE991 greatly enhanced it in *Scn8a*$^{D/+}$ slices (genotype: p=0.024, XE991: p=0.0004, interaction: p=0.039). Statistics were calculated by two-way ANOVA with post hoc Sidak test. **G&H** The effect of I_{KM} activator ICA-110381 (3 μM) was tested in a separate cohort. **G.** In these experiments, SD was detected only in the *Scn8a*$^{D/+}$ cortical tissue and was eliminated by ICA-110381. (genotype: p=0.026, ICA-110381: p=0.026, interaction: p=0.026) **J**. Ca^{2+} spikes in WT and *Scn8a*$^{D/+}$ cortex were also eliminated by ICA-110381. (genotype: p=0.76, ICA-110381: p<0.0001, interaction: p=0.72)

Figure 1

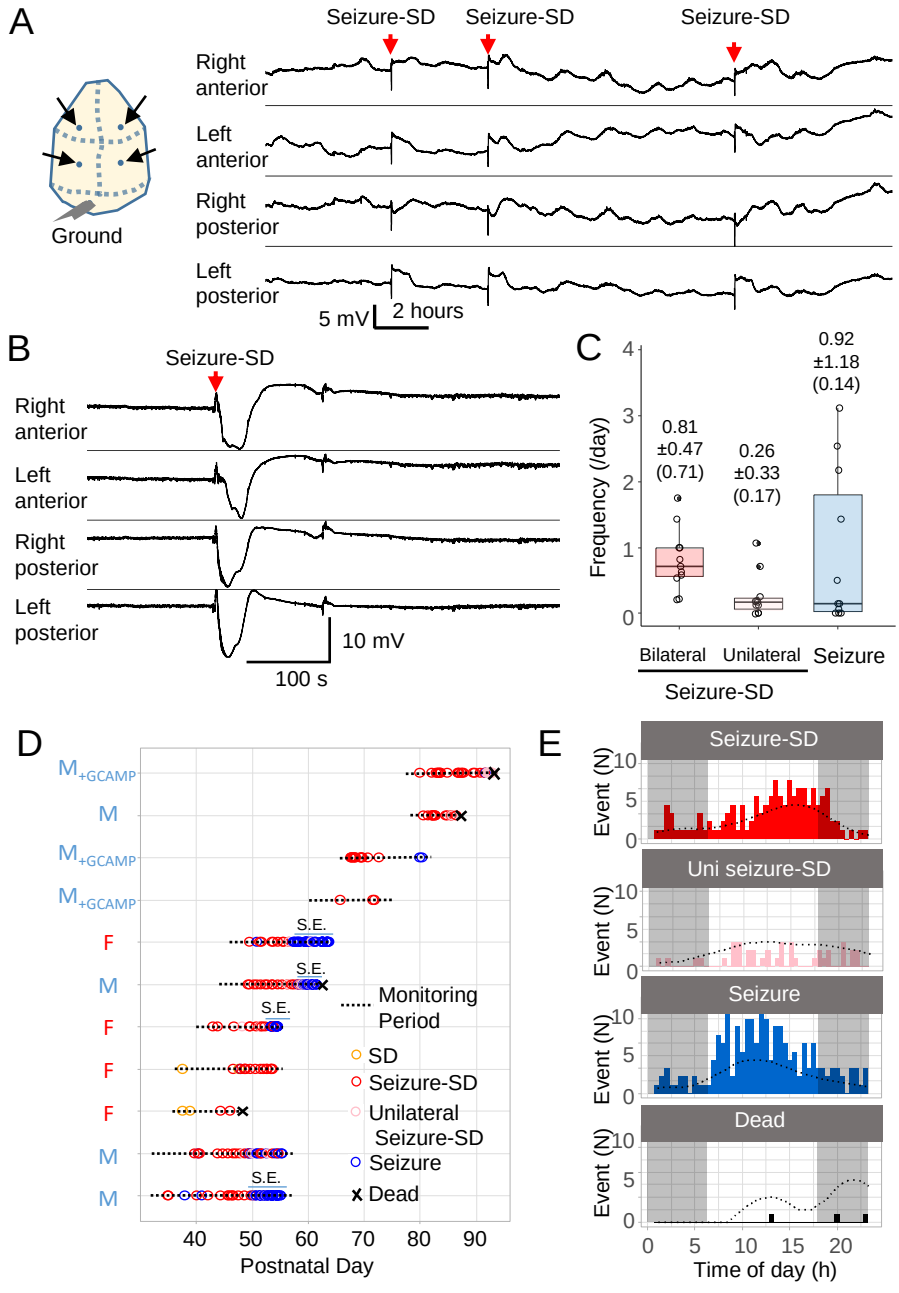
A
Seizure-SD
Seizure-SD
Seizure-SD
Right anterior
Left anterior
Right posterior
Left posterior
Ground
5 mV
2 hours
B
Seizure-SD
Right anterior
Left anterior
Right posterior
Left posterior
10 mV
100 s
C
Frequency (/day)
0.81 ±0.47 (0.71)
0.26 ±0.33 (0.17)
0.92 ±1.18 (0.14)
Bilateral
Unilateral
Seizure
Seizure-SD
D
M+GCAMP
M
M+GCAMP
M+GCAMP
F
M
F
F
F
M
M
S.E.
S.E.
S.E.
S.E.
Monitoring Period
SD
Seizure-SD
Unilateral Seizure-SD
Seizure
Dead
Postnatal Day
E
Seizure-SD
Uni seizure-SD
Seizure
Dead
Event (N)
Time of day (h)

Figure 2

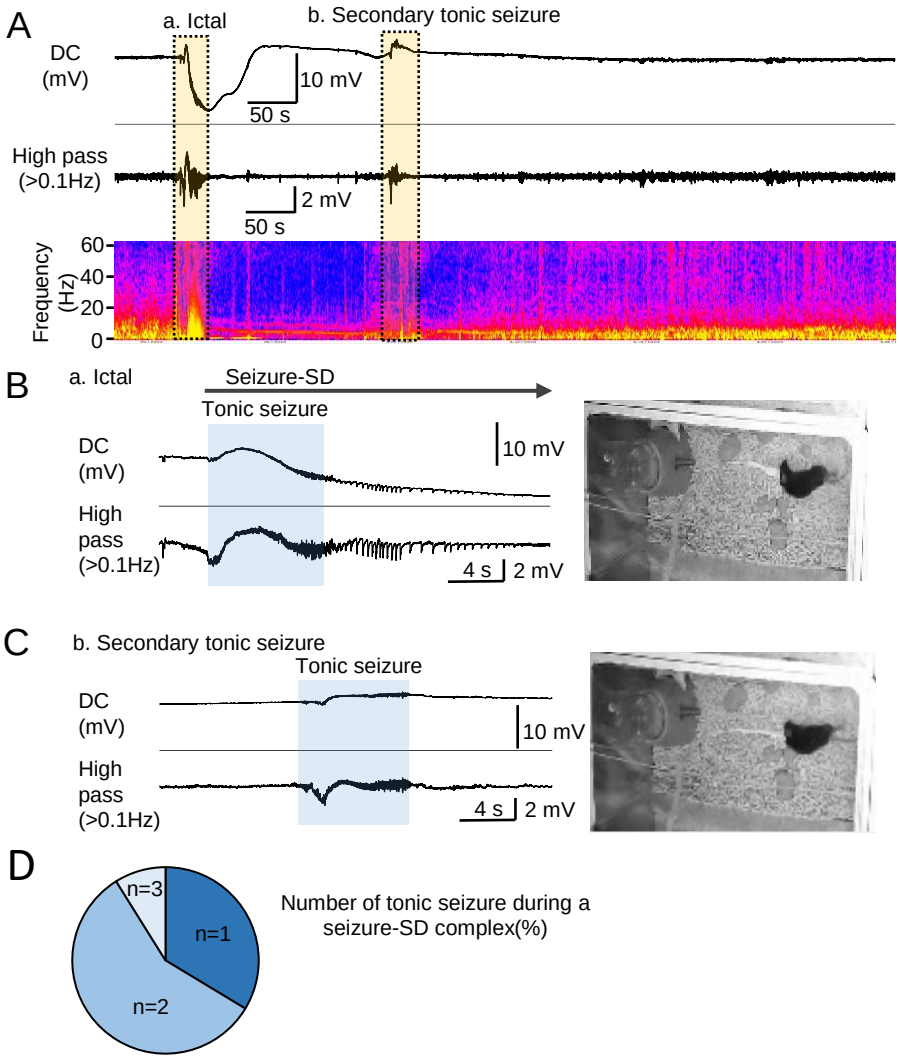
A
a. Ictal
b. Secondary tonic seizure
DC
(mV)
10 mV
50 s
High pass
(>0.1Hz)
2 mV
50 s
Frequency
(Hz)
60
40
20
0
B
a. Ictal
Seizure-SD
Tonic seizure
DC
(mV)
10 mV
High
pass
(>0.1Hz)
4 s
2 mV
C
b. Secondary tonic seizure
Tonic seizure
DC
(mV)
10 mV
High
pass
(>0.1Hz)
4 s
2 mV
D
n=3
n=1
n=2
Number of tonic seizure during a
seizure-SD complex(%)

Figure 3

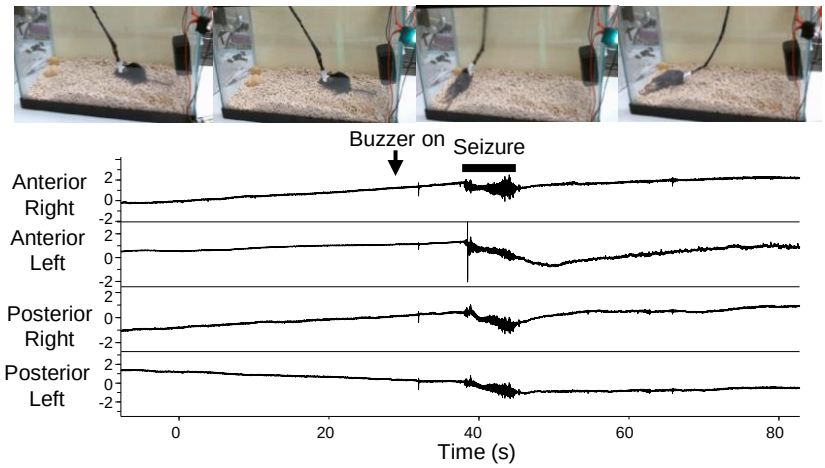
Buzzer on
Seizure
Anterior Right
Anterior Left
Posterior Right
Posterior Left
2
0
-2
0
20
40
60
80
Time (s)

Figure 4

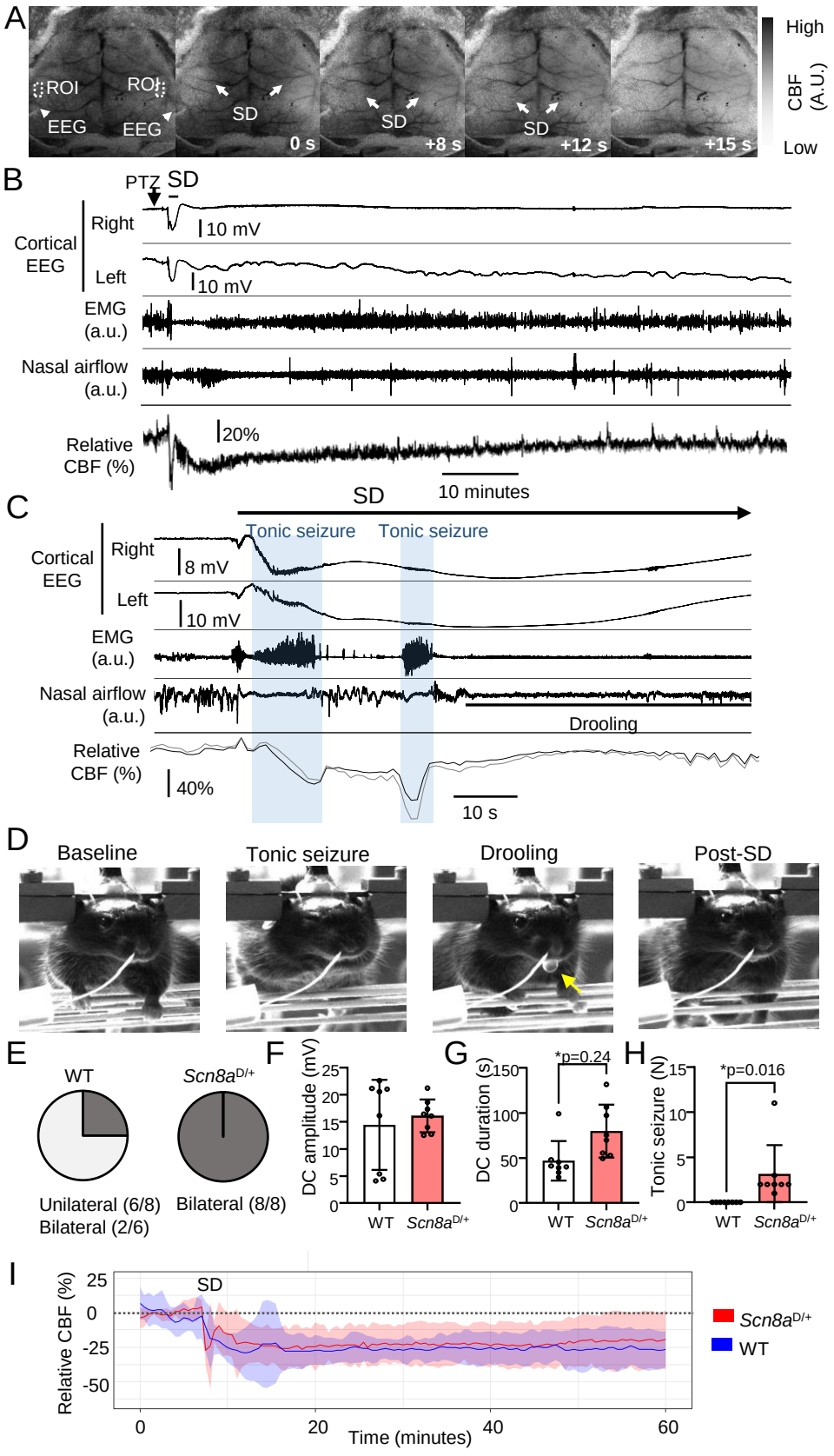
A
ROI
ROI
EEG
EEG
SD
SD
SD
0 s
+8 s
+12 s
+15 s
High
CBF (A.U.)
Low
B
PTZ
SD
Cortical EEG
Right
Left
10 mV
10 mV
EMG (a.u.)
Nasal airflow (a.u.)
Relative CBF (%)
20%
10 minutes
C
SD
Tonic seizure
Tonic seizure
Cortical EEG
Right
Left
8 mV
10 mV
EMG (a.u.)
Nasal airflow (a.u.)
Drooling
Relative CBF (%)
40%
10 s
D
Baseline
Tonic seizure
Drooling
Post-SD
E
WT
Scn8aD/+
Unilateral (6/8)
Bilateral (2/6)
Bilateral (8/8)
F
DC amplitude (mV)
WT
Scn8aD/+
G
DC duration (s)
*p=0.24
WT
Scn8aD/+
H
Tonic seizure (N)
*p=0.016
WT
Scn8aD/+
I
Relative CBF (%)
SD
Time (minutes)
Scn8aD/+
WT

Figure 5

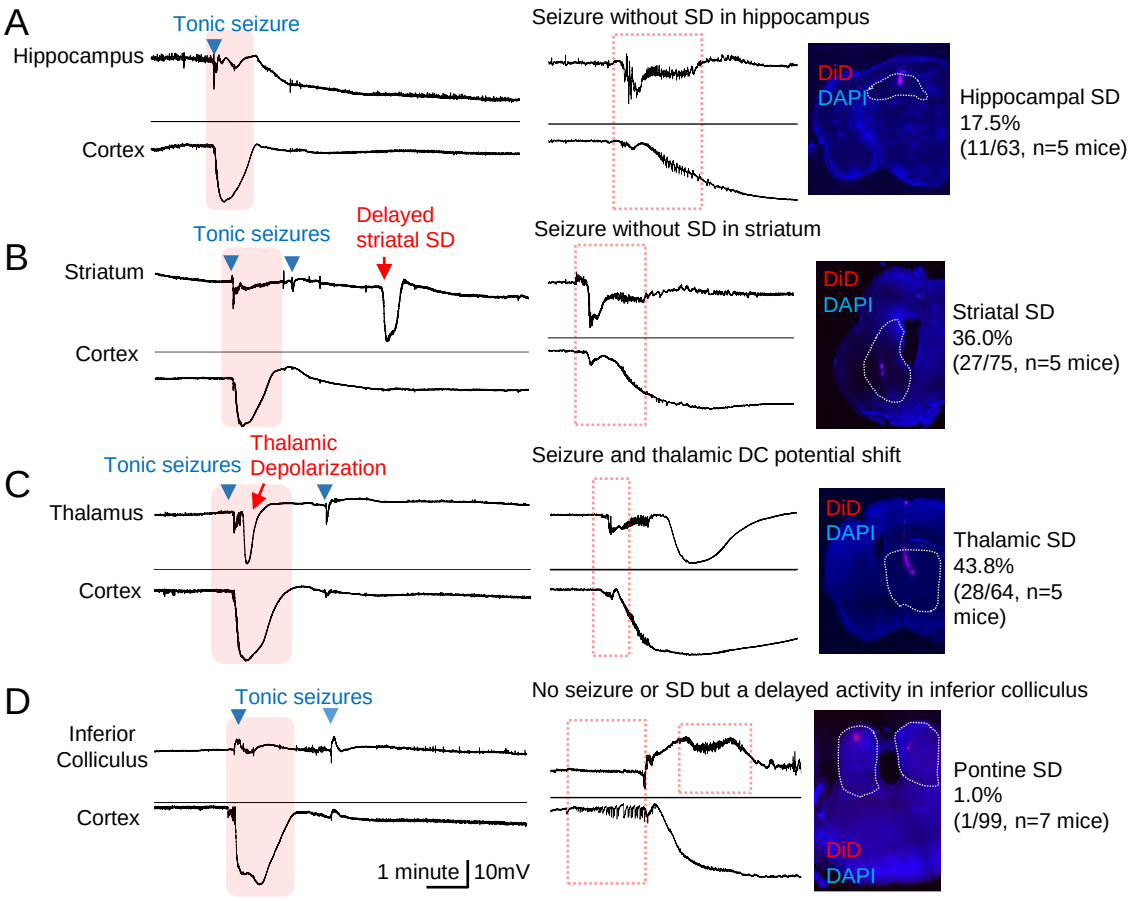
A
Tonic seizure
Hippocampus
Cortex
Seizure without SD in hippocampus
DiD
DAPI
Hippocampal SD
17.5%
(11/63, n=5 mice)
B
Tonic seizures
Delayed
striatal SD
Striatum
Cortex
Seizure without SD in striatum
DiD
DAPI
Striatal SD
36.0%
(27/75, n=5 mice)
C
Tonic seizures
Thalamic
Depolarization
Thalamus
Cortex
Seizure and thalamic DC potential shift
DiD
DAPI
Thalamic SD
43.8%
(28/64, n=5
mice)
D
Tonic seizures
Inferior
Colliculus
Cortex
1 minute
10mV
No seizure or SD but a delayed activity in inferior colliculus
DiD
DAPI
Pontine SD
1.0%
(1/99, n=7 mice)

Figure 6

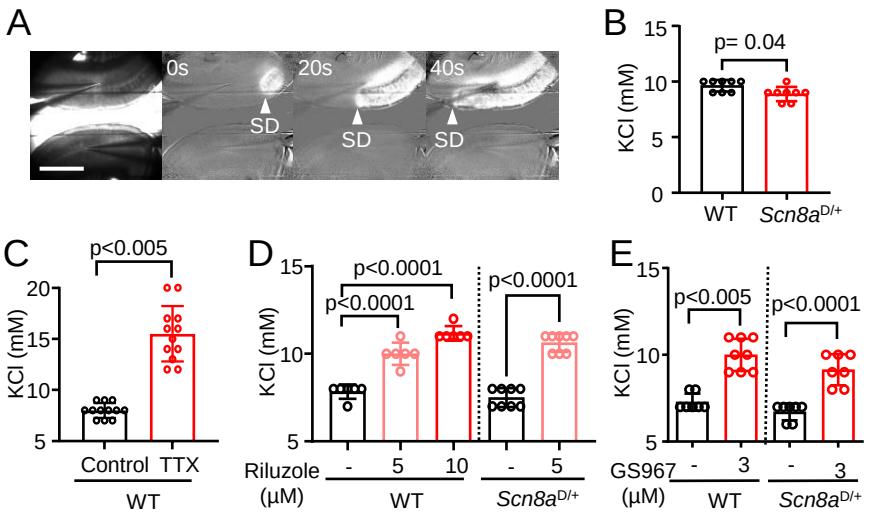
A
0s
20s
40s
SD
SD
SD
B
p= 0.04
KCl (mM)
15
10
5
0
WT
Scn8aD/+
C
p<0.005
KCl (mM)
20
15
10
5
Control
TTX
WT
D
p<0.0001
p<0.0001
p<0.0001
KCl (mM)
15
10
5
Riluzole (μM)
-
5
10
-
5
WT
Scn8aD/+
E
p<0.005
p<0.0001
KCl (mM)
15
10
5
GS967 (μM)
-
3
-
3
WT
Scn8aD/+

Figure 7

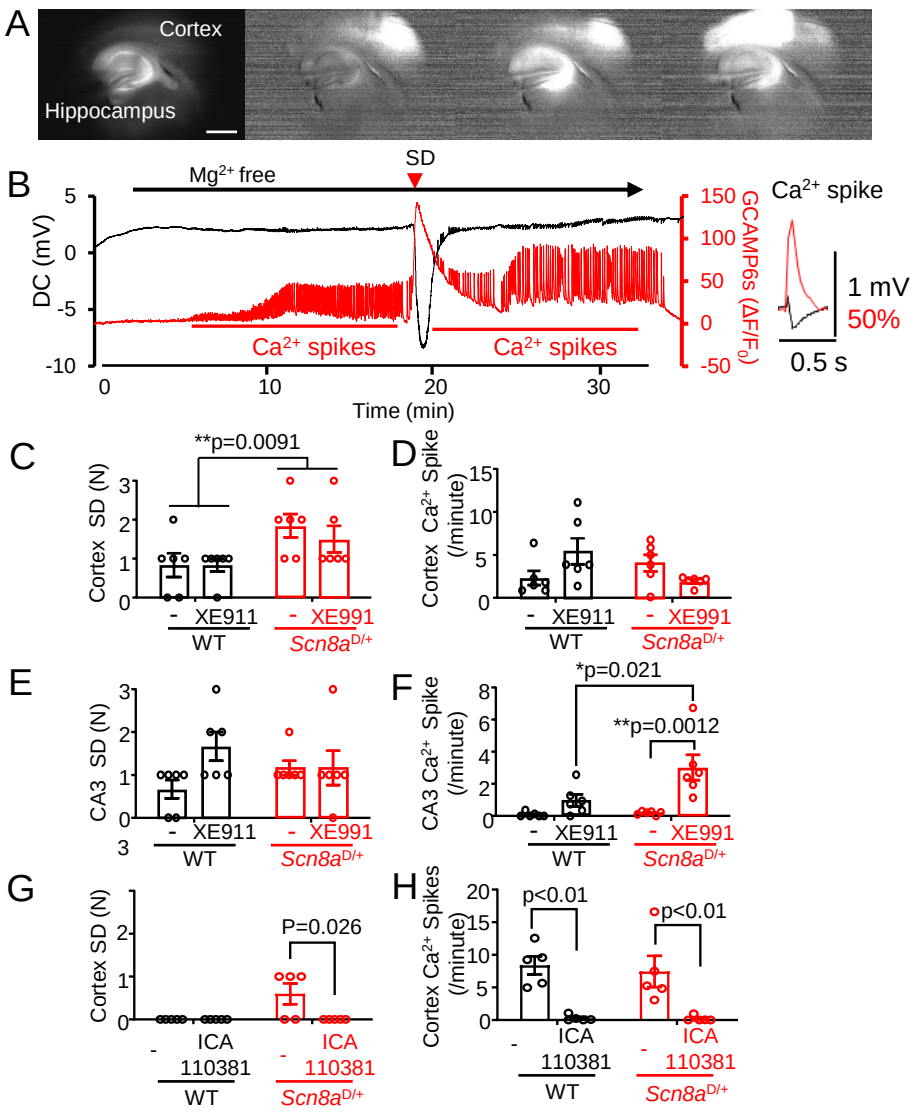
A
Cortex
Hippocampus
B
Mg2+ free
SD
DC (mV)
GCAMP6s (ΔF/F0)
Ca2+ spikes
Ca2+ spikes
Time (min)
Ca2+ spike
1 mV
50%
0.5 s
C
**p=0.0091
Cortex SD (N)
XE911
XE991
WT
Scn8aD/+
D
Cortex Ca2+ Spike (/minute)
E
CA3 SD (N)
F
*p=0.021
**p=0.0012
CA3 Ca2+ Spike (/minute)
G
P=0.026
Cortex SD (N)
ICA 110381
H
p<0.01
p<0.01
Cortex Ca2+ Spikes (/minute)